

# Numerical simulations on flow visualization of blast wave/water wall interaction

Yuta Sugiyama<sup>\*†</sup>, Tomotaka Homae<sup>\*\*</sup>, Kunihiro Wakabayashi<sup>\*</sup>,  
Tomoharu Matsumura<sup>\*</sup>, and Yoshio Nakayama<sup>\*</sup>

<sup>\*</sup>National Institute of Advanced Industrial Science and Technology (AIST),  
Central 5, 1-1-1 Higashi, Tsukuba, Ibaraki 305-8565, JAPAN  
Phone : +81-29-861-0552

<sup>†</sup>Corresponding author : yuta.sugiyama@aist.go.jp

<sup>\*\*</sup>Toyama National College of Technology, 1-2 Ebie-neriya, Imizu, Toyama 933-0293, JAPAN

Received : December 16, 2013 Accepted : February 15, 2014

## Abstract

We developed a multicomponent flow method for three fluids based on a five-equation model by Allaire *et al.* This paper numerically models the experimental results of Homae *et al.* in order to reveal the effect of a barrier material on a blast wave. Three fluids are considered in the present study : the detonation products, water and air, modeled by Jones-Wilkins-Lee (JWL), stiffened gas and ideal gas equations of state, respectively. A water wall was used to encircle a spherical pentolite of 100 g, and the interface problem between the water wall and the blast wave was investigated. To elucidate the effect of the water wall, we conducted two numerical simulations ; one without a water wall and the other with a water wall 100 mm in radius. The peak overpressure, positive impulse and pressure history all agreed well with the experimental results of Homae *et al.* ; thus, our new method is applicable to real explosion phenomena involving multiple fluids. We focused on the interaction of the blast wave with two fluid interfaces (detonation products/water and water/air). Due to the repetitions of reflection and transmission of shock waves at the interfaces, weak shock waves were generated. They reached and affected the propagation of blast wave.

**Keywords** : numerical simulation, multicomponent flow, blast wave, water wall

## 1. Introduction

High energetic explosives are used widely in industrial technologies because even a little explosive releases powerful energy instantly. However, an accidental explosion of high explosives is a hazard to people and has the potential to cause extensive damage to property. Means of minimizing the effects of such an explosion have been investigated for many years. Barrier materials placed around the explosive material have been found to be an effective method for mitigating the effects of the blast wave. Experiments and numerical simulations have been conducted to investigate the suitability of water as a barrier material<sup>1)–4)</sup>. In these studies, it was demonstrated that the maximum peak pressure and impulse were reduced significantly by surrounding the high explosive with a water wall. The internal and kinetic energies of the detonation products are transported into water, which

causes an attenuation of the blast wave. Although some of the attenuation effects of water on blast waves have been investigated experimentally, the attenuation mechanism has not been examined quantitatively because factors such as evaporation and energy exchange make experimental systems complex. Since numerical simulation can provide much available data, it serves as a good alternative to expensive explosion trials with complex physics such as water mitigation, and numerical result is utilized to understand explosion phenomenon quantitatively. Hence, a reliable numerical method for modeling explosion phenomena is very important not only for examining the attenuation effect of a barrier material but for physical hazard analysis in general. In the present paper, to further the development of such methods, we propose a multicomponent flow method for three fluids. The governing equations and algorithm for the method

are described in section 2. In section 3, we validate our method by comparing our numerical data with the previous experimental results of Homae et al. It is shown that our method accurately models blast wave propagation through a water wall.

## 2. Numerical setup

Allaire et al.<sup>5)</sup> proposed a five-equation model (two fluid-mass, one momentum, one energy and one transport) for the simulation of interfaces between compressible fluids under the condition that the pressure and velocity of all fluids remains uniform over time. They validated their model considering two fluids with different equations of state, including the ideal gas, stiffened gas and Mie-Gruneisen equations. We developed a multicomponent flow method for three fluids based on the five-equation model proposed by Allaire et al. In the present study, the detonation products, water, and air are considered in order to reproduce the previous experiment<sup>1)</sup>. Since the previous experiment was conducted under axisymmetric conditions, the governing equations used here are axisymmetric compressible two-dimensional Euler equations (1) and a volume fraction transport equation (2) for the two fluids.

$$\frac{\partial}{\partial t} \begin{bmatrix} \alpha_1 \rho_1 \\ \alpha_2 \rho_2 \\ \alpha_3 \rho_3 \\ \rho v \\ \rho E \end{bmatrix} + \frac{\partial}{\partial x} \begin{bmatrix} \alpha_1 \rho_1 u \\ \alpha_2 \rho_2 u \\ \alpha_3 \rho_3 u \\ \rho u^2 + p \\ \rho uv \end{bmatrix} + \frac{\partial}{\partial y} \begin{bmatrix} \alpha_1 \rho_1 v \\ \alpha_2 \rho_2 v \\ \alpha_3 \rho_3 v \\ \rho uv \\ \rho v^2 + p \end{bmatrix} = -\frac{\rho u}{x} \begin{bmatrix} \alpha_1 \rho_1 / \rho \\ \alpha_2 \rho_2 / \rho \\ \alpha_3 \rho_3 / \rho \\ u \\ v \\ (\rho E + p) / \rho \end{bmatrix} \quad (1)$$

$$\frac{\partial}{\partial t} \begin{bmatrix} \alpha_1 \\ \alpha_2 \end{bmatrix} + u \frac{\partial}{\partial x} \begin{bmatrix} \alpha_1 \\ \alpha_2 \end{bmatrix} + v \frac{\partial}{\partial y} \begin{bmatrix} \alpha_1 \\ \alpha_2 \end{bmatrix} = \begin{bmatrix} 0 \\ 0 \end{bmatrix} \quad (2)$$

Here,  $\alpha_i$  and  $\rho_i$  indicate the volume fraction and density of the  $i$ -th fluid ( $i=1$  for air,  $2$  for water,  $3$  for detonation products).  $u$ ,  $v$ ,  $p$  and  $E$  are the velocities in  $x$  and  $y$  directions, the pressure and the total energy per unit mass, respectively. The ideal gas, stiffened gas and Jones-Wilkins-Lee (JWL) equations of state are used to model air, water and the detonation products, respectively, as shown in Equations (3)–(5).  $\varepsilon_i$  indicate the internal energy per unit mass of the  $i$ -th fluid. Their relation is described in Equation (6). Using conservative variables in Equation (1) and deforming Equations (3)–(6), pressure  $p$  of multicomponent flow is calculated. Here,  $\gamma_1 = 1.4$ ,  $\gamma_2 = 7.15$  and  $\pi = 3.0 \times 10^8$  are chosen as the thermodynamic parameters<sup>6)</sup> in Equations (3) and (4). The JWL parameters listed in Table 1 are used for the detonation products of pentolite<sup>7)</sup>.  $\varepsilon_{30}$  denotes the initial internal energy per unit mass, and  $\varepsilon_3$  is equivalent to  $\varepsilon_{30}$  at initial condition. Relation of sound speed of mixture  $c$  and each fluid  $c_i$  is described in Equation (7).

$$p = (\gamma_1 - 1) \rho_1 \varepsilon_1 \quad (3)$$

$$p = (\gamma_2 - 1) \rho_2 \varepsilon_2 + \gamma_2 \pi \quad (4)$$

**Table 1** JWL parameters of the detonation products of pentolite.

$\rho_0$ [ $\text{kg} \cdot \text{m}^{-3}$ ]	1650
$A$ [GPa]	531.77
$B$ [GPa]	8.933
$R_1$	4.6
$R_2$	1.05
$\omega$	0.33
$\varepsilon_{30}$ [ $\text{MJ} \cdot \text{kg}^{-1}$ ]	4.85

$$p = A \left( 1 - \frac{\omega}{R_1} \frac{\rho_3}{\rho_0} \right) \exp \left( -R_1 \frac{\rho_0}{\rho_3} \right) + B \left( 1 - \frac{\omega}{R_2} \frac{\rho_3}{\rho_0} \right) \exp \left( -R_2 \frac{\rho_0}{\rho_3} \right) + \omega \rho_3 \varepsilon_3 \quad (5)$$

$$\begin{cases} \alpha_1 + \alpha_2 + \alpha_3 = 1 \\ \alpha_1 \rho_1 + \alpha_2 \rho_2 + \alpha_3 \rho_3 = \rho \\ \rho_i E_i = \rho_i \varepsilon_i + \frac{1}{2} \rho_i (u^2 + v^2) \quad (i = 1, 2, 3) \\ \alpha_1 \rho_1 E_1 + \alpha_2 \rho_2 E_2 + \alpha_3 \rho_3 E_3 = \rho E \end{cases} \quad (6)$$

$$\rho \xi c^2 = \sum_i \rho_i \alpha_i \xi_i c_i^2$$

$$\text{where } c_i^2 = \left( \frac{\partial p}{\partial \rho_i} \right)_{\varepsilon_i} + \frac{p}{\rho^2} \left( \frac{\partial p}{\partial \varepsilon_i} \right)_{\rho_i}, \quad \xi_i = \left( \frac{\partial \rho_i \varepsilon_i}{\partial p} \right)_{\rho_i},$$

$$\xi = \sum_i \alpha_i \left( \frac{\partial \rho_i \varepsilon_i}{\partial p} \right)_{\rho_i} \quad (7)$$

In order to simulate interface and blast wave problems, it is important that the numerical scheme correctly models contact surfaces and maintains accuracy with strong shock waves. Additionally, a numerical method should be adaptable to a higher number of fluids; therefore, the numerical flux is expressed by scalars throughout for all conservation equations. This type can be done for Harten-Lax-Leer type (HLL) schemes. The HLL<sup>8)</sup> and HLLC<sup>9)</sup> (HLL-Einfeldt) schemes are very efficient and robust even for strong shock waves and can be applied directly to blast wave problems using the present multicomponent flow method without any modifications. However, the resolution of contact and shear waves can be very inaccurate, and the schemes are not applicable to interface problems. The HLLC (“C” indicates contact) scheme is a modification of the HLL scheme whereby the missing contact and shear waves were restored by Toro *et al.*<sup>10)</sup> The HLLC scheme is the simplest solver that accurately preserves shock, contact, and shear waves over time, but introduces shock instabilities such as the carbuncle phenomenon<sup>11,12)</sup>. The HLLC scheme may not be applicable to strong blast wave problems. To combine the advantages of the two schemes, Kim *et al.*<sup>13)</sup> proposed a control method that applies either the HLL (E) or HLLC scheme to a local flow field. The switching of the HLL (E) and HLLC schemes is determined by the pressure differences between a grid point and the other points around it. This new HLL (E)/HLLC scheme is robust even for strong shock waves and models contact surfaces with high resolution. In the present study, we use the HLL/

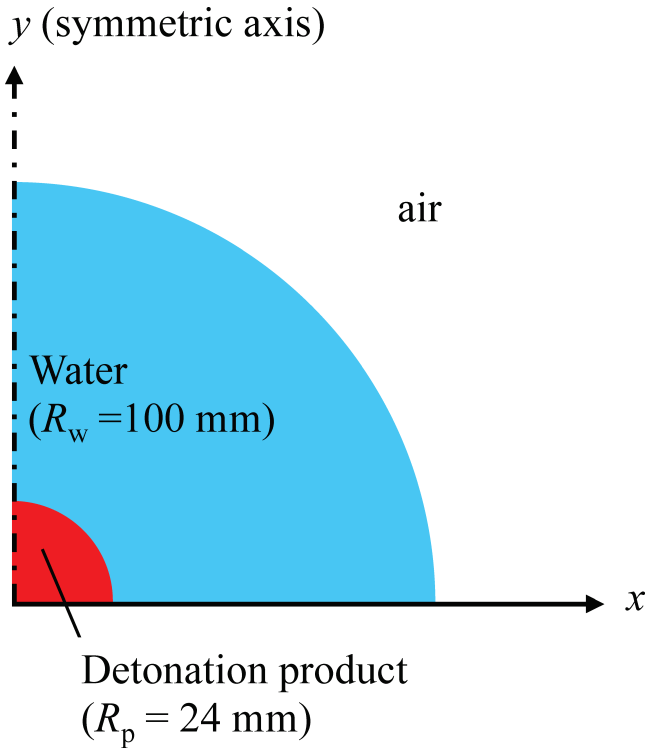


Figure 1 Initial condition with a water wall 100 mm in radius.

HLLC scheme for spatial integration, and conduct 3rd order MUSCL interpolation with a linear scaling limiter<sup>14)</sup>. The 3rd stage TVD Runge-Kutta method<sup>15)</sup> is used for time integration. Figure 1 shows the initial condition including a water wall with an outer radius,  $R_w$ , of 100 mm, encircling the detonation products whose radius and mass are  $R_p = 24$  mm and 100 g, respectively. In this case, the thickness of the water wall is 76 mm. Air is used beyond the water wall. In the experiment, the PMMA container is used to maintain the axisymmetric shape of the explosive. The water wall and the PMMA container may affect the attenuation effect of the blast wave. Therefore, the present study removes the PMMA container since we only discuss the attenuation effect of a water wall.

The computational grid is orthogonal with constant spacing. Mirror boundaries are employed along the  $x$ - and  $y$ -axes in order to reduce the computational cost. In a numerical simulation of explosion and blast wave propagation, the grid resolution is often determined by the number of grid points in a scaled distance  $K$ ,  $\text{m kg}^{-1/3}$ . In the present study, the scaled distance of  $1 \text{ m kg}^{-1/3}$  corresponds to 464 mm, so 464 grid points per the scaled distance are set in all directions ( $\Delta x = \Delta y = 1.0$  mm). Figure 2 shows the peak overpressure distribution of the hemispherical explosion of pentolite of 100 g by two-dimensional axisymmetric calculation without a water wall. The distribution compares with an empirical curve of TNT by Kingery and Bulmash<sup>16)</sup>. Here, because the chemical energy of pentolite is larger than that of TNT, the scaled distance was corrected considering the initial internal energies of pentolite  $\epsilon_{\text{Pen}} = \epsilon_{30} = 4.85 \text{ MJ kg}^{-1}$  and TNT  $\epsilon_{\text{TNT}} = 4.2 \text{ MJ kg}^{-1}$  as  $K^* = K / (\epsilon / \epsilon_{\text{TNT}})^{1/3} \text{ m kg}^{-1/3}$ . We confirmed that the peak overpressure agrees well with the empirical curve. This indicates that the grid resolution

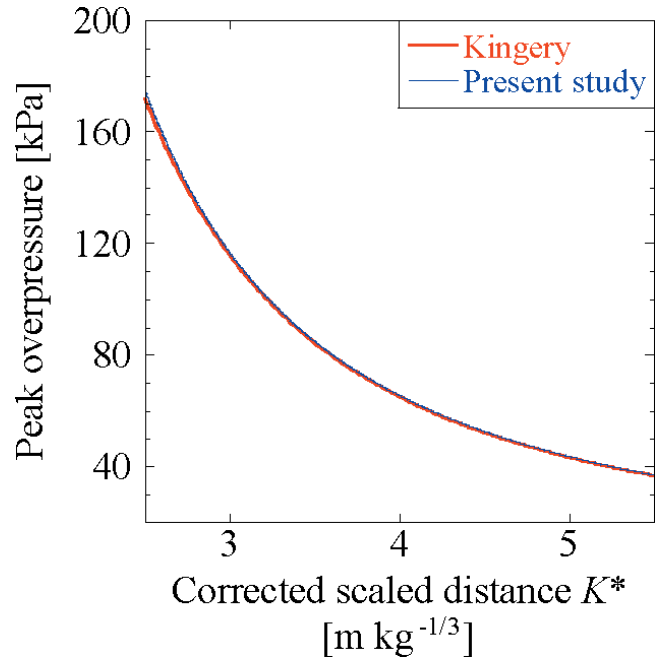
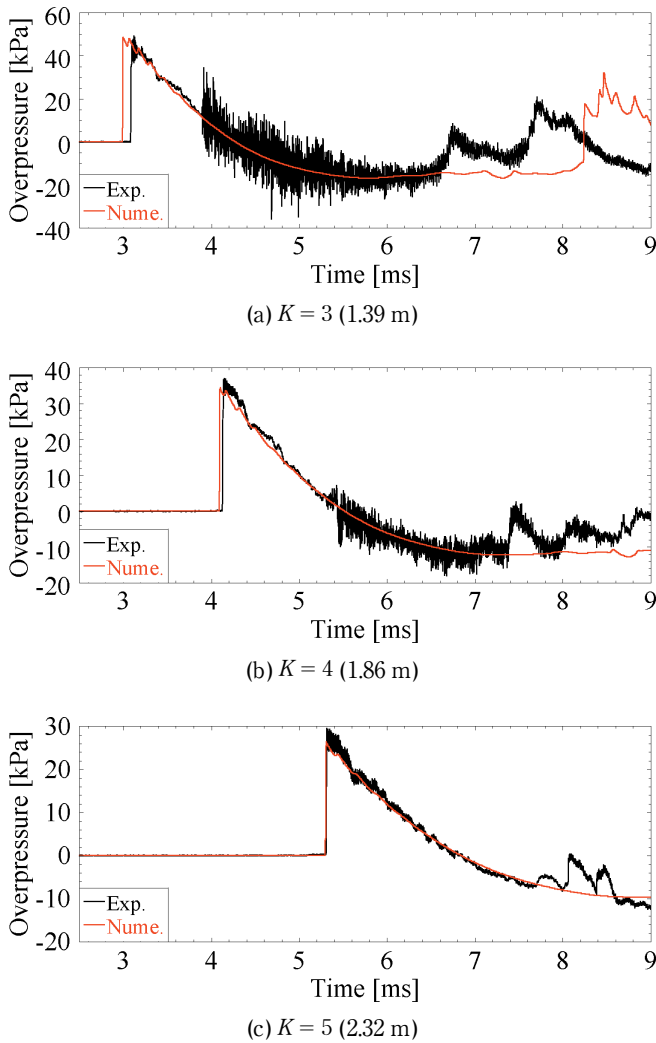


Figure 2 Peak overpressure distributions of the hemispherical explosion in the present study (pentolite,  $\epsilon = \epsilon_{\text{Pen}}$ ) and the empirical curve (TNT,  $\epsilon = \epsilon_{\text{TNT}}$ ) of Kingery. The horizontal axis indicates the corrected scaled distance  $K^* = K / (\epsilon / \epsilon_{\text{TNT}})^{1/3}$ .

is sufficient to accurately calculate the explosion and blast wave propagation.

### 3. Results

Our data, as well as those from the experiments of Homae *et al.*, incorporates a scaled distance  $K$ ,  $\text{m kg}^{-1/3}$ . The experimental data were fitted using a spline function. The peak pressure and positive impulse are determined from the fitted curve<sup>1)</sup>. Figure 3 shows the pressure histories for (a)  $K = 3$ , (b)  $K = 4$ , and (c)  $K = 5$  in the case of a water wall of 100 mm. The overpressure suddenly increases due to the blast wave and then decreases gradually. In the experiment, high-frequency pressure oscillation occurred, the cause of which was considered to be fragments of a PMMA container colliding with pressure transducers. The characteristics of the pressure histories, namely, the time of arrival of the blast wave, the peak overpressure and the decay curve, show good agreement with the previous experimental results. Figure 4 describes the enclosed view around the blast wave arrival of Figure 3(a). and shows the weak pressure oscillations after the first peak of overpressure in the present numerical simulation. Figure 5 denotes (a) the peak overpressure and (b) the normalized peak overpressure distributions. The plots and curves show the results of the experiments and the numerical simulation, respectively. Peak overpressures are normalized with respect to those in the case without water. The present study shows that the attenuation effect decreases with the increment of the scaled distance. In the present study, normalized peak overpressure stays constant around 0.8 at  $K \geq 5$ . This indicates that the attenuation effect maintains over a wide range from the explosion center. There is a difference of 10 % in the peak overpressure



**Figure 3** Pressure histories for (a)  $K = 3$ , (b)  $K = 4$  and (c)  $K = 5$  with a water wall of 100 mm.

between the experiments and the numerical simulations. It would appear that our simulation does not consider the PMMA container to maintain the axisymmetric shape of the explosive in the experiment. In the case with the water wall, there are some points at which the gradient of the peak overpressure in Figure 5 (a) changes locally. We utilize the normalized peak overpressure in Figure 5 (b) to estimate the attenuation effect of the water wall on the blast wave. The normalized peak overpressure in the present numerical simulation agrees well with that of the previous experiment and increases with the scaled distance increments. Figure 6 shows (a) positive impulses and (b) normalized positive impulse distributions. Positive impulses are normalized with respect to those in the case without water. They also show good agreement between the experiment and the numerical simulation. Therefore, it can be concluded that our developed numerical method accurately models the results of explosions and blast wave propagation through a water wall.

As mentioned above, Figure 4 shows that weak pressure oscillations occur after the first peak of overpressure, and Figure 5 (a) shows local gradient changes at some points. In this paper, we discuss the associated mechanism in terms of flow patterns. Figure 7 shows snapshot of the absolute value of density gradient

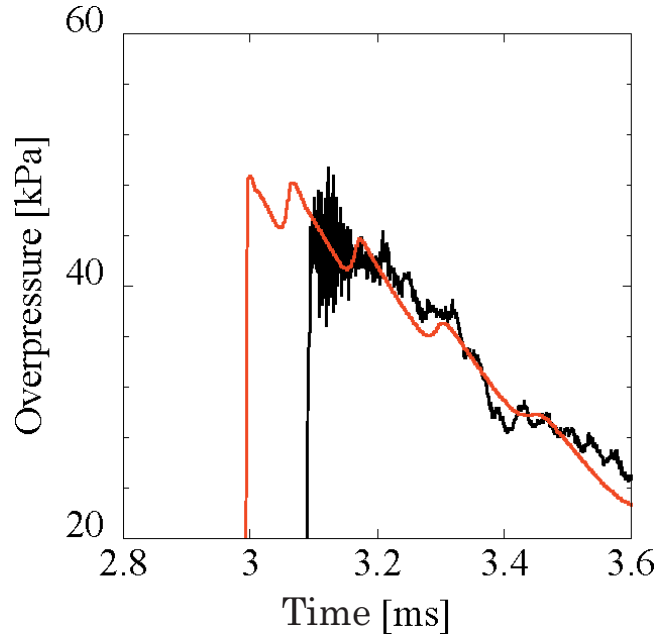


**Figure 4** Enclosed view around the blast wave arrival of Figure 3 (a).

distribution at  $t = 1.5$  ms on the  $x-y$  plane. In Figure 7, the blast wave is located at  $1.7 \text{ m kg}^{-1/3}$ , and the white lines either side of the black belt around  $1.2 \text{ m kg}^{-1/3}$  indicate the interfaces between the fluids (detonation products/water and water/air). Many shock waves between the blast wave and water/air interface are visible. Figure 8 shows (a) snapshot of the absolute value of density gradient distribution on the  $x-t$  plane at  $y=0$ , and (b) schematic picture of reflection and transmission of waves at detonation products/water and water/air interfaces. We confirmed that flow characteristics are independent of lines at  $y=0$ ,  $y=x$ , and others. As shown in the  $x-t$  diagram of Figure 8 (a), they are periodically generated not only at the water/air interface propagating to the blast wave, but also at the detonation products/water interface propagating to the explosion center ( $x=0$ ). The time taken for an acoustic wave propagating at  $1,464 \text{ m/s}$  in water of  $76 \text{ mm}$  to travel back and forth is  $0.104 \text{ ms}$ . This value agrees well with the averaged period of  $0.114 \text{ ms}$  between 0 and  $1.5 \text{ ms}$  at which shock waves are generated at the water/air interface. This indicates that the repetitions of reflection and transmission of the shock waves at the detonation/water and water/air interfaces induce successive shock waves shown as transmitted wave in Figure 8 (b), and they propagate to the blast wave and result in the pressure oscillations shown in Figure 4. When they reach the blast wave at  $K = 2.3$  and  $2.8 \text{ m kg}^{-1/3}$  as shown in Figure 8 (a), the gradient of the peak overpressure changes locally as in Figure 5 (a). The reflection and transmission are important to elucidate the attenuation effect of the barrier material and the propagation mechanism of the blast wave.

#### 4. Conclusion

This paper proposes a multicomponent flow method for three fluids. We validated our method for modeling a blast wave problem attenuated by a water wall. Air, water and

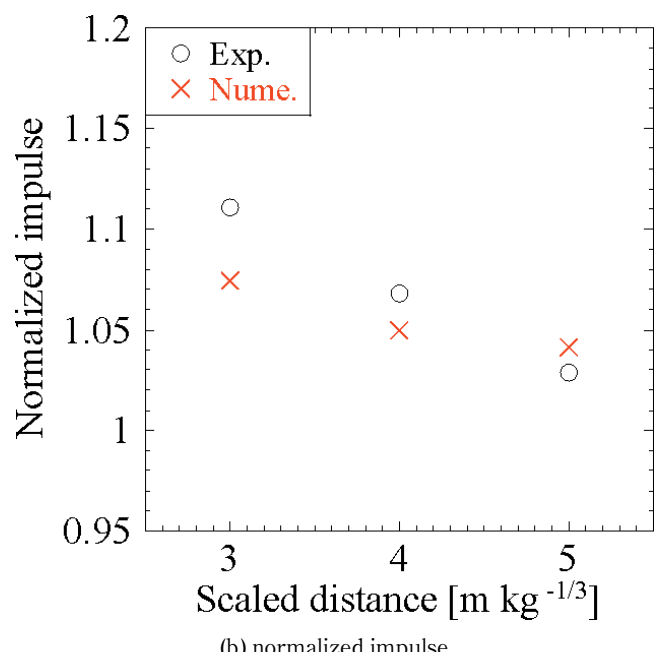
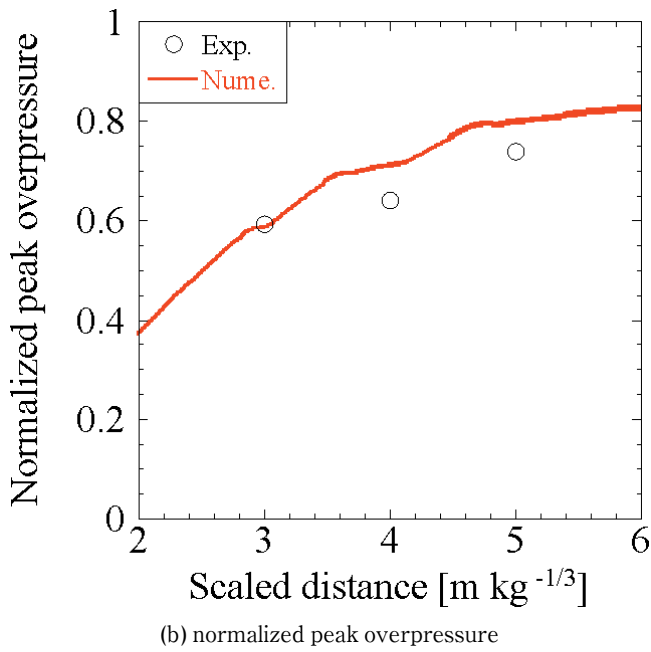
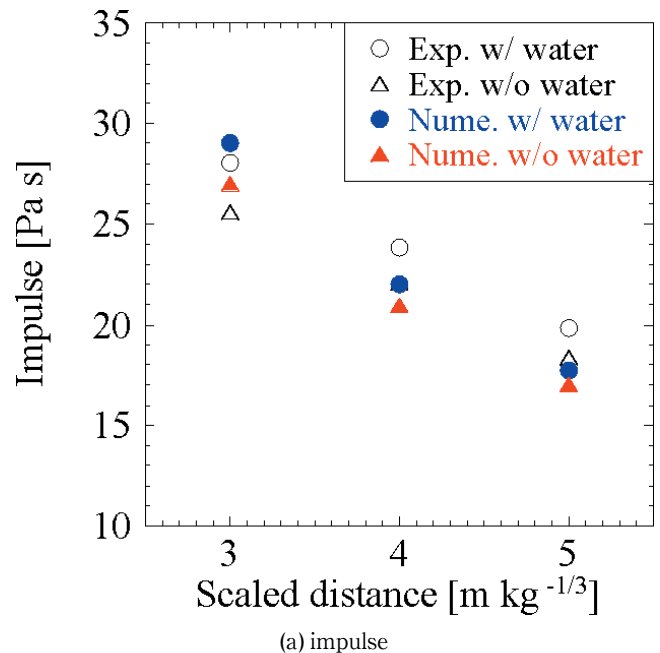
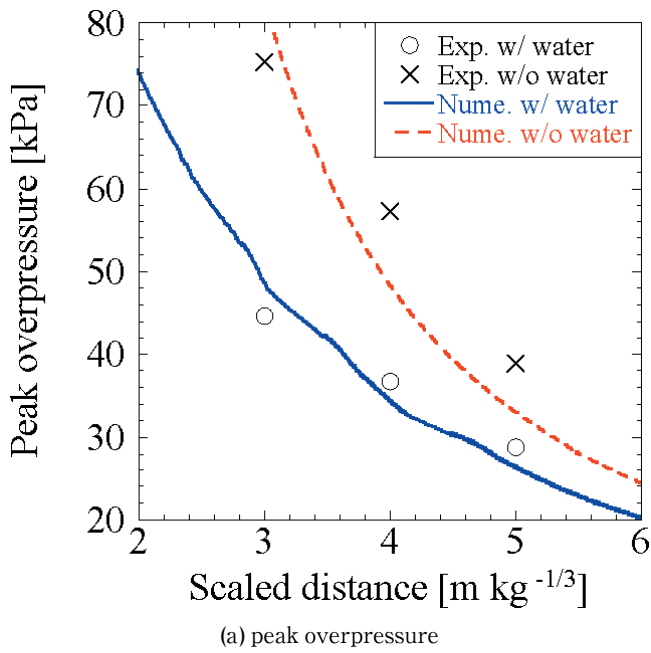


**Figure 5** Comparison of the present study with the experiment; (a) the peak overpressure and (b) the normalized peak overpressure distributions. Peak overpressures are normalized with respect to those in the case without water.

**Figure 6** Comparison of the present study with the experiment; (a) the impulse and (b) the normalized impulse distributions. Positive impulses are normalized with respect to those in the case without water.

the detonation products were modeled by the ideal gas, the stiffened gas and the JWL equations of state, respectively. Our numerical data were compared with the experimental results of Homae *et al.* It was shown that our method accurately models the peak overpressure and impulse when the blast wave is attenuated by a water wall. The repetitions of reflection and transmission of the shock waves at the fluid interfaces affect the propagation of the blast wave and are important factors for elucidating the attenuation effect of the water wall.

**Reference**

1) T. Homae, K. Wakabayashi, T. Matsumura, and Y.

Nakayama, *Sci. Tech. Energetic Materials*, 67, 182–186 (2006) (in Japanese).  
 2) W. A. Keenan and P. C. Wager, *Proc. the 25th DoD Explosives Safety Seminar*, 311–339 (1992), Anaheim, CL, USA.  
 3) M. Cheng, K. C. Hung and O. Y. Chong, *Shock Waves* 14, 217–223 (2005).  
 4) Y. S. Shin, M. Lee, K. Y. Lam and K. S. Yeo, *Shock Vibr.* 5, 225–234 (1998).  
 5) G. Allaire, S. Clerc and S. Kokh, *J. Comput. Phys.* 181, 577–616 (2002).  
 6) T. Gallouët, J. M. Hérard and N. Seguin, *Internat. J. Numer. Methods Fluids* 39, 1073–1138 (2002).

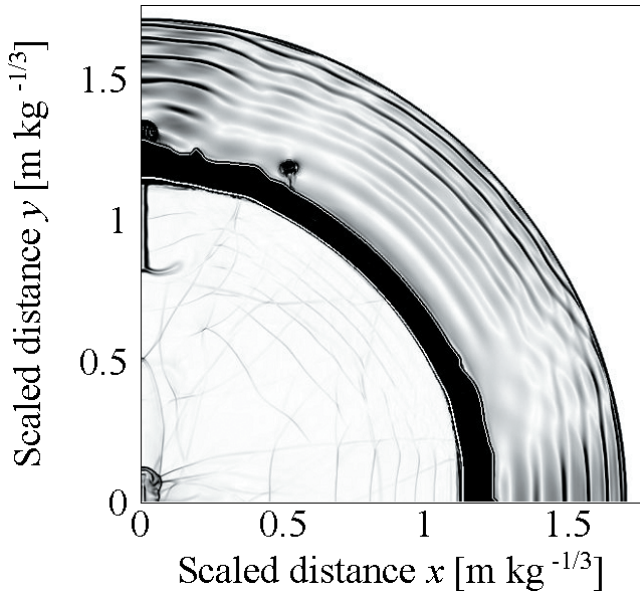


Figure 7 Snapshot of the absolute value of density gradient distribution at 1.5 ms.

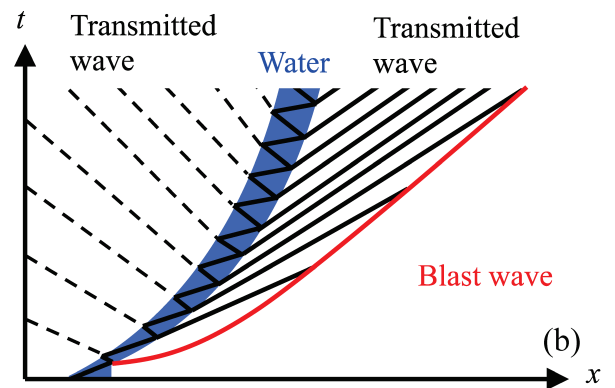
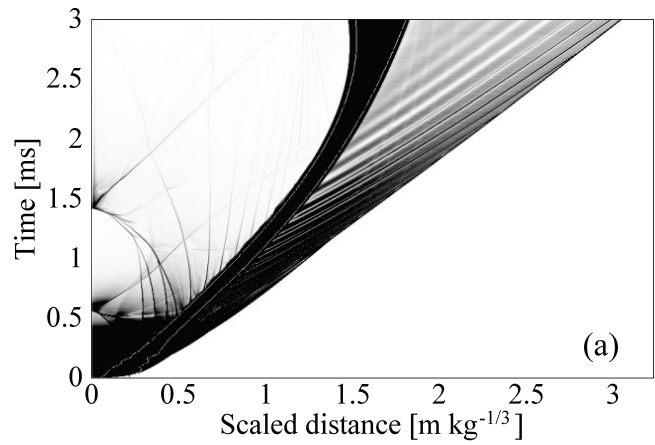


Figure 8 (a) Absolute value of density gradient distribution in the  $x-t$  plane at  $y=0$  and (b) schematic picture of reflection and transmission of waves.

- 7) J. P. Lu, J. G. Anderson and F. C. Christo, Proc. the 24th Int. Symp. on Shock Waves, 855–860 (2004), Beijing, China.
- 8) A. Harten, P. D. Lax and B. van Leer, SIAM Review 25, 35–61 (1983).
- 9) B. Einfeldt, SIAM J. Numer. Anal. 25, 294–318 (1988).
- 10) E. F. Toro, M. Spruce and W. Speares, Shock Waves 4, 25–34 (1994).
- 11) M.-S. Liou, J. Comput. Phys. 160, 623–648 (2000).
- 12) M. Pandolfi and D. D'Ambrosio, J. Comput. Phys. 166, 271–301 (2001).
- 13) S. D. Kim, B. J. Lee, H. J. Lee, I.-S. Jeung and J.-Y. Choi, Int. J. Numer. Meth. Fluids 62, 1107–1133 (2010).
- 14) X. Zhang and C.-W. Shu, Proc. R. Soc. A 467, 2752–2776 (2011).
- 15) C.-W. Shu and S. Osher, J. Comput. Phys. 77, 439–471 (1988).
- 16) C. N. Kingery and G. Bulmash, ARBRL-TR-02555, Ballistics Research Laboratory (1984).

# 爆風と水の干渉の可視化に関する数値解析

杉山勇太<sup>\*†</sup>, 保前友高<sup>\*\*</sup>, 若林邦彦<sup>\*</sup>, 松村知治<sup>\*</sup>, 中山良男<sup>\*</sup>

爆風低減メカニズムの解明を目的として, Allaireらの手法を改良した多種流体を考慮した数値計算手法を開発した。本稿では, 障害物の影響を解明するために爆ごう生成ガス, 水, 空気の三流体を用いて保前らの実験を再現した。本計算では半径24mmの球形ペントライト100gの爆ごう生成ガスの周りを水で覆い, 爆風と水の干渉問題を数値解析によって再現した。水の有無による影響を調査するため, 水なし及び半径100mmの水がある場合をそれぞれ数値解析した。本数値解析と実験は最大過圧, インパルスと爆風の圧力履歴が実験と良い一致を示したことから, 爆風については開発した本手法で実験を再現できると考えられる。また, 爆風の伝播メカニズムとして水と空気界面における爆風の反射と透過の影響に着目した。2つの流体界面における爆風の反射と透過が繰り返されることによって微弱な衝撃波が発生し, それが爆風に到達することによって爆風伝播に影響を与えることがわかった。

\*独立行政法人 産業技術総合研究所 〒305-8565 茨城県つくば市東1-1-1 中央第五  
Phone: 029-861-0552

†Corresponding author: yuta.sugiyama@aist.go.jp

\*\*富山高等専門学校 〒933-0293 富山県射水市海老江練合1-2